Polymer 55 (2014) 2481–2490

Contents lists available at ScienceDirect

Polymer

journal homepage: www.elsevier.com/locate/polymer

# Phase transformation and self-assembly behavior of supramolecular rod–comb block copolymers

Yi-Huan Lee [a,b], Chun-Jie Chang [a], Yi-Lung Yang [a], Chi-Ju Chiang [b], Yu-Ping Lee [b], Ching Shen [b], Kang-Ting Tsai [c], Yi-Fan Chen [d], Chi-An Dai [a,b,*]

[a] Institute of Polymer Science and Engineering, National Taiwan University, Taipei 10617, Taiwan
[b] Department of Chemical Engineering, National Taiwan University, Taipei 10617, Taiwan
[c] Program of Landscape and Recreation, National Chung Hsing University, Taichung 40227, Taiwan
[d] Department of Chemical and Materials Engineering, National Central University, Jhongli 32001, Taiwan

ARTICLE INFO

*Article history:*
Received 15 November 2013
Received in revised form
17 January 2014
Accepted 31 January 2014
Available online 14 March 2014

*Keywords:*
Macroterminator
Rod–comb block copolymer
Hierarchical structure

ABSTRACT

We investigated the self-assembly behavior of a series of supramolecular rod–comb block copolymer complexes made by the hybridization of rod–coil diblock copolymers of poly (2,5-di(2-ethylhexyloxy)-1,4-phenylene vinylene)-*b*-poly(2-vinyl pyridine) (PPV-*b*-P2VP$_f$) with different volume fractions, *f*, of the P2VP coils and an anionic surfactant, dodecyl benzenesulfonic acid (DBSA), that selectively interacts with the P2VP to form the side-chain comb teeth. The resulting hybrids show hierarchically ordered structures at multiple length scales, forming so-called structure-in-structure morphology. Notably, for PPV-*b*-P2VP$_{0.56}$(DBSA)$_x$, the larger-scale structure changes from a lamellar phase, to a broken lamella, and eventually to a hexagonally packed strip phase with increasing DBSA molar ratio ($x$) to P2VP monomer unit. Furthermore, simultaneous SAXS and WAXS measurements showed that the order-disorder transition temperatures of larger-scale structures in the PPV-P2VP$_{0.56}$(DBSA) rod–comb systems were higher than those associated with the pristine PPV-P2VP$_{0.56}$ polymers. The large-scale structure of PPV-P2VP$_{0.56}$(DBSA) exists at temperatures around 210 °C even though the rod–rod interaction between PPV blocks disappear at ~120 °C, signifying that the formation of the P2VP(DBSA) lamellar mesophase plays a critical role in forming the large-scale hexagonally packed strip structures.



## 1. Introduction

Block copolymers have now emerged as a new class of important smart materials for both academic study and industrial application over the past decades owing to their ability to self-assemble into structures with feature sizes ranging from several nanometers to hundreds of nanometers [1–6]. Traditional coil–coil block copolymers can form a variety of ordered morphologies depending on several parameters such as the volume fraction ($f$), Flory–Huggins interaction parameter ($\chi$), and the degree of polymerization ($N$) of the copolymers. Typical ordered morphologies for the coil–coil diblock copolymers include body-centered-cubic packed spheres (BCC), hexagonally packed cylinders (HPC), bicontinuous gyroids (G), and the lamellar phase (L).

Recently, π-conjugated rod–coil block copolymers have received a great deal of attention in materials science and nanotechnology [7–15] since they can be used as active materials in organic electronics such as organic field-effect transistors (OFETs) [16,17] and organic photovoltaic cells (OPV) [18,19]. The π-conjugated rigid-rod backbone may induce novel microstructures that are significantly different from those of conventional random coil-based block copolymers. It was found that the phase behavior of a rod–coil system is governed not only by the aforementioned molecular parameters of $f$, $\chi$, and $N$, but also by the liquid crystalline interaction between the rod blocks characterized by the Maier–Saupe interaction parameter, $\mu$, as well as by the molecular packing between the rod and coil blocks [20,21]. Therefore, the interplay between these parameters may create morphologies that are different from that of the classical coil–coil block copolymer system such as zig-zag, wavy lamellar, arrow-head [22,23], smectic-A like lamellar [24], hexagonal strip [25–27], and puck phases. [27–29].

In addition, a new class of comb-shaped supramolecules consisting of flexible or mesogenic side chains that bind to the

* Corresponding author. No. 1, Roosevelt Rd. Sec. 4, Department of Chemical Engineering, National Taiwan University, Taipei 10617, Taiwan. Tel.: +886 2 33663051; fax: +886 2 23623040.
*E-mail address:* polymer@ntu.edu.tw (C.-A. Dai).

http://dx.doi.org/10.1016/j.polymer.2014.01.056
0032-3861/

backbone polymer chains via ionic bonding, hydrogen bonding, or metal-mediated coordination bonding has recently been fabricated [30–42]. By having one particular block of a diblock copolymer selectively interacts with surfactants or oligomeric amphiphiles, complicated hierarchical supramolecular structures of the resulting hybrid may be observed, showing ordered morphologies at multiple length scales. One advantage of using the diblock copolymer to form the hierarchical structure is to facilitate the formation of the comb-shaped architecture via the supramolecular approach in which the short chain molecules are attached to the copolymer backbone. The self-assembly behavior of the supramolecular comb–coil complex block copolymers with hierarchical structures have received significant attention due to its potential for use as a new approach for fabricating functional materials in electrical, optical, and other applications [43–50]. In hierarchical comb–coil systems, the larger self-assembled structure that results from the repulsive interaction between the comb and coil blocks usually has the domain size in the range of several tens of nanometers, while the smaller structure is formed through the polar-nonpolar repulsion interaction between the backbone and side chains of the comb block that induces the formation of a lamellar mesophase with a characteristic length on the order of several nanometers.

The self-assembly behavior of the supramolecular comb-shaped complexes formed by coil–coil diblock copolymers with different architectures such as linear, heteroarm star, and block-arm star copolymers has been thoroughly studied [32–35]. In the present study, we are interested in studying a supramolecular rod–comb block copolymer complex consisting of an amphiphilic surfactant and a π-conjugated rod–coil block copolymer. The π–π interaction between the rod blocks offers a different microphase separation behavior since the strong π–π interaction of the rod blocks with liquid crystalline ordering characteristics often dominates the phase behavior of rod–coil block copolymer systems, leading to the formation of a lamellar phase over a wide range of copolymer composition which results in a highly asymmetric phase diagram [51–54]. Hence, the liquid crystalline interaction may also have considerable effects on the phase behavior of the supramolecular rod–comb complexes compared to that of the coil–comb complexes. This may result in interesting and novel, self-organized morphologies, in addition to phase transitions.

Therefore, the objective of the current study is to investigate how the side-chain comb teeth molecules influence the self-assembled structure and phase transitions of rod–comb block copolymers. We present a novel rod–comb block copolymer system by blending an anionic surfactant, dodecyl benzenesulfonic acid (DBSA) with a rod–coil block copolymer of poly(2,5-di(2-ethyl hexyloxy)-1,4-pheny-lenevinylene)-block-poly(2-vinyl pyridine) (PPV-*b*-P2VP). Two different rod–coil block copolymers of PPV-*b*-P2VP$_{f=0.3}$ and PPV-*b*-P2VP$_{f=0.56}$, in which $f$ is the volume fraction of P2VP block in the neat copolymers, were used to study the effects of copolymer composition, the rod–rod interaction between PPV blocks, and the amount of DBSA, on their resulting morphology. In particular, the effect of temperature on the self-assembly and phase transformation of the rod–comb block copolymer was studied. In contrast to the supramolecular comb-shaped complexes formed by the coil–coil diblock copolymer systems, different morphological transitions were found in the series, which are strongly related to their rod–rod interactions. By a combination of transmission electron microscopy (TEM) and simultaneously measured small-angle and wide-angle X-ray scattering (SAXS and WAXS) measurements on the PPV-*b*-P2VP(DBSA)$_x$ supramolecular complexes (with $x$ denoting the average number of DBSA molecules bound with 2-vinyl pyridine monomer unit), we discuss in detail the effect of DBSA composition on the rod–rod interaction between poly(2,5-di(2′-ethylhexyloxy)-1,4-phenylene vinylene) (DEH-PPV) chains and on the formation of the resulting microstructures.

## 2. Experimental section

### 2.1. Materials

A macroterminator of aldehyde end-functionalized DEH-PPV was synthesized by Seigrist polycondensation as shown in Scheme 1 [53,55]. The synthesis routes and characterization of DEH-PPV are described in the Supporting Information. All reactions were carried out under purified nitrogen. Ultrahigh purity nitrogen was purchased (purity of 99.9995%) and further purified by passing it through a column of molecular sieves and a BTS (Fluka) catalytic oxygen trap. Tetrahydrofuran (Mallinckrodt, 99%, THF) was freshly distilled after being refluxed with excess sodium metal and benzophenol (Acros, 99%) for use as an indicator for dryness. *sec*-Butyllithium (Chemetal, 1.3 M in cyclohexane) was used as an initiator for the anionic polymerization. 2-Vinyl pyridine (2VP, Acros, 97%) monomer was purified by stirring the monomer in a flask with calcium hydride for several days followed by purification using a freeze-thaw technique with trioctyl aluminum (Aldrich, 25% solution in hexane) as the drying agent before polymerization. Dodecylbenzene sulfonic acid (DBSA, Fluka, 90%) was dried in vacuum at 60 °C for 24 h before use.

### 2.2. Synthesis of poly(2,5-di(2′-ethylhexyloxy)-1,4-phenylene vinylene)-block-poly(2-vinylpyridine) (PPV-b-P2VP)

The synthesis procedure for the PPV-*b*-P2VP is shown in Scheme 2. Anionic polymerization of 2-vinylpyridine was performed in THF. *sec*-Butyllithium was used to initiate the 2VP to form poly(2-vinylpyridine) anions at −78 °C, and an aliquot of poly(2-vinylpyridine) homopolymer was collected and terminated with dry methanol to measure its molecular weight and polydispersity. The anionic polymerization was allowed to react for 3 h. A macroterminator of aldehyde end-functionalized DEH-PPV (1.5 equiv) was dried under vacuum at room temperature overnight, then dissolved in THF, and transferred to couple with the living P2VP anions. The obtained PPV-*b*-P2VP block copolymers were purified using either the precipitation or extraction method.

*PPV-b-P2VP$_{0.3}$* $^1$H NMR (400 MHz, $CDCl_3$, ppm): $\delta$ 8.20 (*d*, 1.66H, Ar −N=C*H*−), 7.43–7.17 (*m*, 5.66H), 6.79 (*br*, 1.66H), 6.30 (*br*, 1.66H, −C$H_3$−), 3.88–3.64 (*m*, 4H, −OC$H_2$−), 2.29–1.27 (*m*, 22.97H), 0.85 (br, 12H). PDI: 1.12.

*PPV-b-P2VP$_{0.56}$* $^1$H NMR (400 MHz, $CDCl_3$, ppm): $\delta$ 8.20 (*d*, 4.77H, Ar −N=C*H*−), 7.44–7.17 (*m*, 8.77H), 6.79 (*br*, 4.77H), 6.29 (*br*, 4.77H), 3.87–3.62 (*m*, 4H, −OC$H_2$−), 2.31–1.29 (*m*, 32.30H), 0.87 (br, 12H, −C$H_3$). PDI: 1.12.

### 2.3. Characterization

The molecular weight distribution of the synthesized block copolymers were measured by using a GPC (Waters 2695) equipped with two Styragel columns (HR3 and HR4E), a refractive index detector (Waters 2414) and a photodiode array absorbance detector (Waters 2996). THF was used as the mobile phase at a flow rate of 1 mL/min and monodispersed polystyrene standards (Pressure Chemicals) were used for system calibration. The synthesized block copolymers were dissolved in $CDCl_3$ and their 1H NMR spectra were recorded on a 400 MHz Bruker Avance spectrometer at room temperature. NMR spectra were reported in ppm. Splitting patterns were designated as *d* (doublet), *m* (multiplet), and *br* (broad resonance).

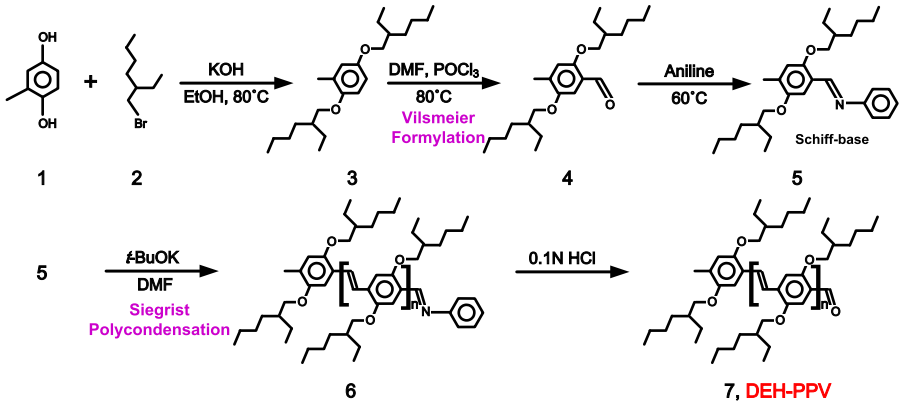


**Scheme 1.** Synthetic routes of aldehyde end-functionalized DEH-PPV.

### 2.4. Sample preparation for rod–comb diblock copolymers

PPV-*b*-P2VP(DBSA)$_x$ rod–comb diblock copolymer hybrid, where $x$ denotes the molar ratio of DBSA molecules to 2-vinyl pyridine monomer units, were prepared by dissolving PPV-*b*-P2VP and DBSA in dichloromethane ($CH_2Cl_2$), a good solvent for both DEH-PPV and P2VP blocks. The concentration of the neat block copolymer was maintained at 5wt% to ensure homogeneous solution formation. The solution was stirred for 24 h and subsequently evaporated slowly at room temperature. After the solvent was evaporated, the samples were further dried in a vacuum oven at 40 °C for 1 day to remove any residual solvent.

### 2.5. Simultaneous small-/wide-angle X-ray scattering (SAXS/WAXS) measurement

Simultaneous SAXS/WAXS experiments were performed at the beamline 23A1 of National Synchrotron Radiation Research Center (NSRRC) in Taiwan. The dried hybrid samples were sealed in washers of 1.0 mm in thickness and 0.25 mm in diameter, and Kapton® films were used as windows for the X-rays. Before the scattering experiment, all samples were annealed in the high vacuum oven ($10^{-6}$ torr) at 120 °C for 24 h. A two-dimensional MAR CCD with 1024 × 1024 channels for the SAXS measurements and a one-dimensional gas-type linear detector for the WAXS measurements were used to collect the scattering patterns. The molecular characteristics of the complexes are summarized in Table 2.

### 2.6. Transmission electron microscopy (TEM)

The morphology of neat PPV-*b*-P2VP copolymers and PPV-*b*-P2VP(DBSA)$_x$ complexes annealed using the same thermal treatment process as the samples for the SAXS/WAXS experiments were determined by using a JEOL JEM-1230 operated at an accelerating voltage of 120 kV. Ultrathin sections (approximately 70 nm) of PPV-*b*-P2VP were microtomed at room temperature by using Leica Ultracut UCT6 machine. The more hygroscopic PPV-*b*-P2VP(DBSA)$_x$ samples were cryomicrotomed at −90 °C. Thin sections were collected onto 200-mesh copper grids coated with carbon-supporting films. To enhance contrast of the DEH-PPV domains, $RuO_4$ stained the sections for 30 min.

## 3. Results and discussion

### 3.1. Synthesis of PPV-b-P2VP by coupling living P2VP anion chain with an end-functional macroterminator

A series of PPV-*b*-P2VP block copolymers were synthesized by coupling the aldehyde end-functionalized DEH-PPV rods of $M_n$ = 3800 with P2VP living anion chains of different molecular weights synthesized by using the anionic polymerization. Before coupling with DEH-PPV, the molecular weight characteristics of P2VP were measured using gel permeation chromatography (GPC). The polydispersity index (PDI) of all P2VP samples was less than 1.15. To ensure a complete coupling reaction of the transferred P2VP living anions with the aldehyde end-functionalized PPVs, an excess amount of DEH-PPV (1.5 mol equiv) to the P2VP anions was used. According to the composition of PPV-*b*-P2VP block copolymer, unreacted DEH-PPV can be removed by using an extraction method as described below. Since hexane is a good solvent for DEH-PPV but a poor one for P2VP, copolymers with coil fractions near or larger than the symmetric composition can be easily separated from the copolymer/homopolymer mixture solution by using hexane as the extraction solvent at the ambient temperature. However, as the

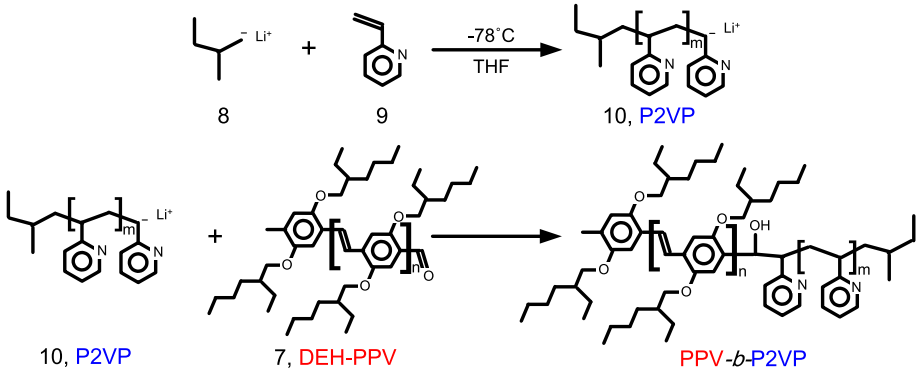


**Scheme 2.** Synthetic routes of PPV-*b*-P2VP block copolymers.

**Table 1**
Molecular characteristics of PPV-*b*-P2VP block copolymers.

| Block copolymers | $M_n$ (g/mol) DEH-PPV[a] | $M_n$ (g/mol) P2VP[a] | PDI[a] | $f$[b] P2VP | Morphology |
|---|---|---|---|---|---|
| PPV-*b*-P2VP$_{0.3}$ | 3800 | 1600 | 1.16 | 0.30 | lamella |
| PPV-*b*-P2VP$_{0.56}$ | 3800 | 4800 | 1.14 | 0.56 | lamella |

[a] From GPC.
[b] Volume fraction of P2VP.

copolymer with coil fractions significantly lower than the symmetric composition was synthesized, the copolymer could not be separated from the mixture solution at room temperature. Instead, it could be selectively precipitated in hexane at low temperature (~−78 °C). After cooling the solution for at least five times for purification, the PDI and the molecular weight of the PPV-*b*-P2VP block copolymer precipitates were evaluated by GPC and $^1$H NMR, measurements.

The GPC traces for PPV-*b*-P2VP$_{0.56}$ and its precursor homopolymers are shown in Fig. 1. The chromatograph of the as-synthesized PPV-*b*-P2VP$_{0.56}$ exhibits two peaks: one for the unreacted DEH-PPV homopolymer and one for the coupled PPV-*b*-P2VP$_{0.56}$ block copolymer. The number-average molecular weight ($M_n$ = 3800) of the aldehyde end-functionalized DEH-PPV block was determined using NMR end-group analysis by the comparison of the aldehyde proton peak with the $-OCH_2$ peak. Alternately, based on the $^1$H NMR spectrum in Fig. 2, the mole fraction of DEH-PPV block in PPV-*b*-P2VP$_{0.56}$ (~17%) was calculated by integrating the area ratio between the $-OCH_2-$ signal ($\delta$ = 3.6–3.9 ppm) of the alkoxy side-chain of DEH-PPV and the aromatic −N−*CH*− signal ($\delta$ = 8.0–8.4 ppm) of P2VP. The volume fraction of P2VP in the synthesized PPV-*b*-P2VP sample was calculated to be 0.56. Therefore, the PPV-*b*-P2VP block copolymer was denoted as PPV-*b*-P2VP$_{0.56}$. The results of the molecular weight characterization of the copolymers are listed in Table 1.

### 3.2. Hierarchical structures of the rod–comb complexes

At first, we report the details on the morphological investigation of the thermally annealed supramolecular rod–comb complexes by employing TEM and SAXS. Fig. 3a shows the SAXS profiles for the PPV-*b*-P2VP$_{0.3}$(DBSA)$_x$ hybrids. For $x$ = 0, the neat PPV-*b*-P2VP$_{0.3}$ block copolymer exhibited a highly ordered lamellar structure with scattering peaks at integer multiples of the primary scattering peak ($q^*$). Based on the Braggs' equation, the long period is estimated to be 9.1 nm for the neat PPV-*b*-P2VP$_{0.3}$ block copolymer. As the loading ratio increased from $x$ = 0 to $x$ = 0.5, and eventually to $x$ = 1.0, the presence of a lamellar phase in this hybrid system remained unchanged as verified by their SAXS profiles with peak position ratio of 1:2. With increasing DBSA loadings, the long period of the lamellar structure for the hybrid as determined from

**Table 2**
Molecular characteristics of PPV-*b*-P2VP(DBSA)$_x$ rod–comb supramolecular complex.

| Rod–comb block copolymers | $x$[a] | $f_{P2VP+DBSA}$[b] | Long period (nm) | Morphology |
|---|---|---|---|---|
| PPV-*b*-P2VP$_{0.3}$(DBSA)$_x$ | 0 | 0.3 | 9.1 | lamellae-in-lamellae |
| | 0.5 | 0.52 | 14.6 | lamellae-in-lamellae |
| | 1.0 | 0.64 | 15.6 | lamellae-in-lamellae |
| PPV-*b*-P2VP$_{0.56}$(DBSA)$_x$ | 0 | 0.56 | 14.2 | lamellae-in-lamellae |
| | 0.5 | 0.72 | 18.0 | lamellae-in-lamellae |
| | 1.0 | 0.81 | 14.3 | strips-in-lamellae |

[a] Number of DBSA molecules per vinyl pyridine repeating unit.
[b] Overall volume fraction of P2VP and DBSA in the copolymers.

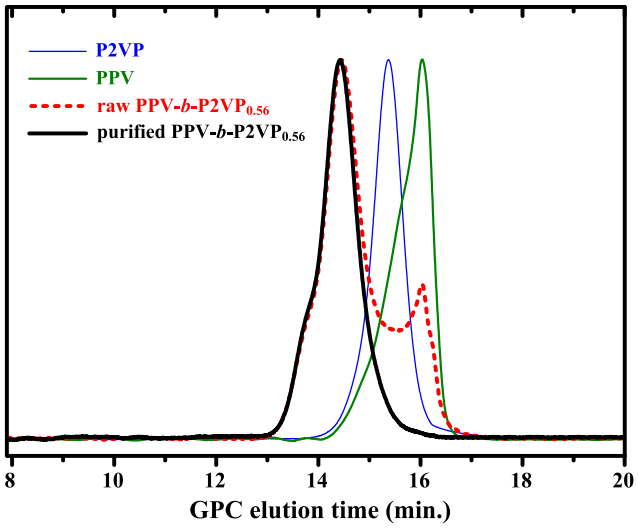


**Fig. 1.** The GPC traces of P2VP precursor (blue line), aldehyde end-functionalized DEH-PPV homopolymer (green line), as-synthesized PPV-*b*-P2VP$_{0.56}$ (red dash line), and purified PPV-*b*-P2VP$_{0.56}$ block copolymer (black line). (For interpretation of the references to color in this figure legend, the reader is referred to the web version of this article.)

the first scattering peak values $q^*$ increased from 9.1 nm for $x$ = 0, to 15.6 nm for $x$ = 1.0. It is considered that the increase in the domain spacing is due to the chain-stretching effect upon the introduction of DBSA complexed with P2VP blocks [34,35]. Therefore, the domain spacing of the lamellar structure increased with the bonding fraction of DBSA to P2VP.

Additionally, in the high-$q$ range of the SAXS profiles shown in Fig. 3a, a new peak located at 2.1 nm$^{-1}$ emerges (as indicated by a dotted arrow), and the intensity of the peak increases with increasing DBSA loading. The presence of the new peak specifies the formation of a small-scale lamellar mesophase organized by P2VP(DBSA) comb blocks which improves the alignment between P2VP chains in their domain, leading to the emergence of the new peak. Based on the Braggs' equation, the domain spacing of the small-scale lamellar structure is found to be equal to 3 nm. Therefore, the PPV-*b*-P2VP$_{0.3}$(DBSA)$_{1.0}$ rod–comb hybrid exhibits a structure-within-structure morphology in which DEH-PPV and P2VP(DBSA) layers were alternatively arranged normal to the

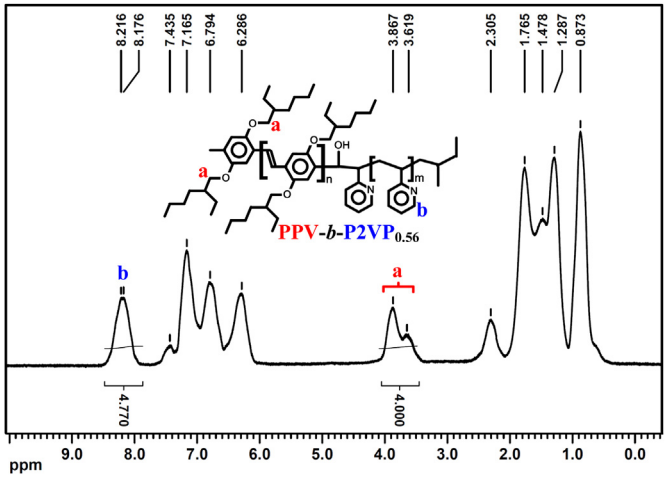


**Fig. 2.** $^1$H NMR spectrum of PPV-*b*-P2VP$_{0.56}$ block copolymer in $CDCl_3$.

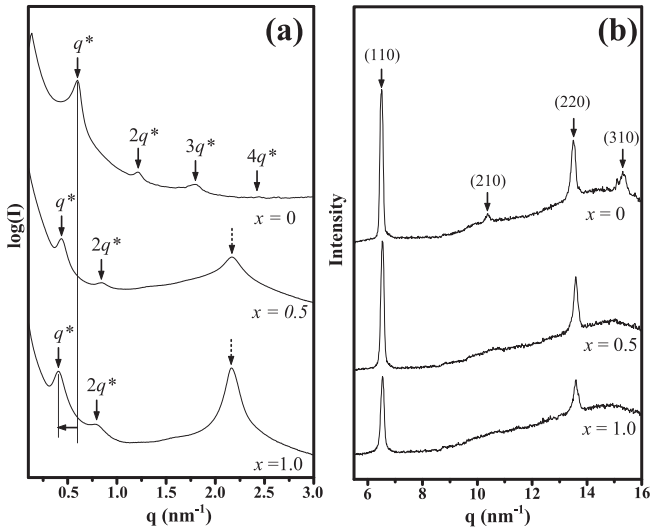


**Fig. 3.** The evolution of (a) SAXS and (b) WAXS patterns as a function of the number of DBSA molecules per vinyl pyridine repeating unit for the PPV-*b*-P2VP$_{0.3}$(DBSA)$x$ complex.

domain surface. As a result, the way that DEH-PPV, P2VP, as well as DBSA pack within their domain for the PPV-*b*-P2VP$_{0.3}$(DBSA)$_x$ system with $x = 0$ and $x = 1$ can be schematically illustrated by Scheme 3(a) and (b), respectively. The effect of DBSA composition on the crystalline structure of the hybrid is investigated by using WAXS measurements. The assignment for the crystalline plane of each diffraction peak shown in all the WAXS spectra is based on a previous X-ray study on the DEH-PPV homopolymer by Segalman et al. [56] We also consistently observed (110), (210), (220), and (310) diffraction planes from DEH-PPV in the neat PPV-*b*-P2VP$_{0.3}$. As shown in Fig. 3b, the first peak matched with the (110) plane

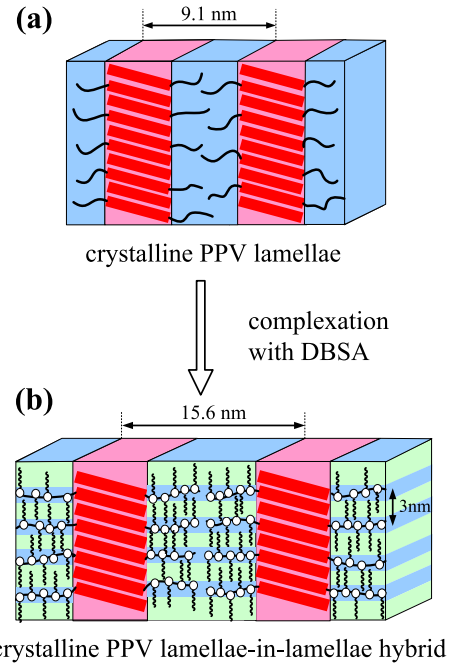


**Scheme 3.** (a) The lamellar morphology formed in the neat PPV-*b*-P2VP$_{0.3}$ rod–coil block copolymer and (b) hierarchical structure formed in PPV-*b*-P2VP$_{0.3}$(DBSA)$_{1.0}$ wherein the lamellar layers of DEH-PPV are embedded in the lamellar mesophase formed by P2VP(DBSA) comb blocks.

located at around 6.5 nm$^{-1}$ corresponds to the lateral spacing between the DEH-PPV rods, which gives the molecular diameter of the DEH-PPV rod of ~0.97 nm, with its peak magnitude decreasing with increasing DBSA fractions. Even though the total volume fraction of P2VP(DBSA) increased from 0.3 for the neat PPV-*b*-P2VP block copolymer to a value of 0.6 for the PPV-*b*-P2VP$_{0.3}$(DBSA)$_{1.0}$ hybrid, the characteristic (110) peak position which represents the distance between DEH-PPV rods remain unchanged.

However, it can be expected that the chain-stretching effect of both P2VP and DBSA chains would increase the free energy of the complex system due to the loss of conformation entropy in the hybridized P2VP(DBSA) domains. Therefore, this complex system may undergo morphological transition to reduce its free energy by increasing defects within the otherwise long-range straight DEH-PPV lamellae and form a so-called broken lamellar structure to avoid the excessive chain stretching of P2VP blocks [57]. TEM micrographs of the PPV-*b*-P2VP$_{0.3}$(DBSA)$_x$ hybrid system can provide important information about how PPV-*b*-P2VP and DBSA might be organized within their nanodomains as a function of different DBSA fractions. Fig. 4a shows a transmission electron micrograph of the neat PPV-*b*-P2VP$_{0.3}$ stained with $RuO_4$. The DEH-PPV domain shown as the dark phase in the micrograph exhibits a highly ordered and long-range lamellar structure. With increasing DBSA fraction from $x = 0.5$ to $x = 1.0$, their TEM images are shown in Fig. 4b and c, respectively, illustrating that the long-range order of lamellae disappears, resulting in broken lamellae. This evolution is similar to the observation in many previous studies of weakly segregated rod–coil block copolymer systems with an increase in their effective coil volume fraction [52,53,57].

The phase behavior of the PPV-*b*-P2VP(DBSA)$_x$ hybrid system is further studied by changing the neat copolymer composition. For the P2VP-rich PPV-*b*-P2VP$_{0.56}$ block copolymer, the molecular weight of its P2VP block is increased significantly compared with that of P2VP block in PPV-*b*-P2VP$_{0.3}$, while the molecular weight of DEH-PPV block remain roughly constant for the two samples. The corresponding SAXS patterns of PPV-*b*-P2VP$_{0.56}$(DBSA)$_x$ are shown in Fig. 5a. Similar to the morphology of the neat PPV-*b*-P2VP$_{0.3}$ block copolymer, PPV-*b*-P2VP$_{0.56}$ also shows a large-scale morphology exhibited as a lamellar structure with SAXS scattering peaks located at integer multiples of the primary scattering peak ($q^*$). Subsequently, as the DBSA fraction $x$ was increased from $x = 0$ to $x = 0.5$, the PPV-*b*-P2VP$_{0.56}$(DBSA)$_{0.5}$ hybrid still adopts a self-assembled lamellar structure and the position of the first-order scattering peak in the SAXS profiles decreasing with increasing DBSA fractions from $x = 0$ to $x = 0.5$, indicating an increase in the long period of the lamellar phase from 14.2 nm for $x = 0$, to 18 nm for $x = 0.5$.

For the volume fraction typical in the range of 0.2–0.3, conventional coil–coil diblock copolymers often adopt a self-assembled hexagonal close packed cylindrical structure (HCP). However, by treating DBSA as a selective solvent to the P2VP domains to obtain a combined volume fraction of DBSA and P2VP of 0.28, PV-*b*-P2VP$_{0.56}$(DBSA)$_{0.5}$ system still adopts a rather long range ordered lamellar structure. Therefore, the formation of the lamellar phase in the PPV-*b*-P2VP$_{0.56}$(DBSA)$_{0.5}$ hybrid indicates that the rod–rod interaction between DEH-PPV rods plays a critical role to prevent the formation of nanostructures with a curved interface. Furthermore, TEM can be used to provide important information about how PPV-*b*-P2VP$_{0.56}$(DBSA)$_{0.5}$ might be organized within its nanostructure. PPV-*b*-P2VP$_{0.56}$(DBSA)$_{0.5}$ stained in the DEH-PPV domain with $RuO_4$ exhibits only disrupted and short-range dark lines of the DEH-PPV domain with its morphology shown in Fig. 4e. This is in great contrast to that of the neat PPV-*b*-P2VP$_{0.56}$ block copolymer shown in Fig. 4d, whereby a long-range ordered lamellar structure was observed.

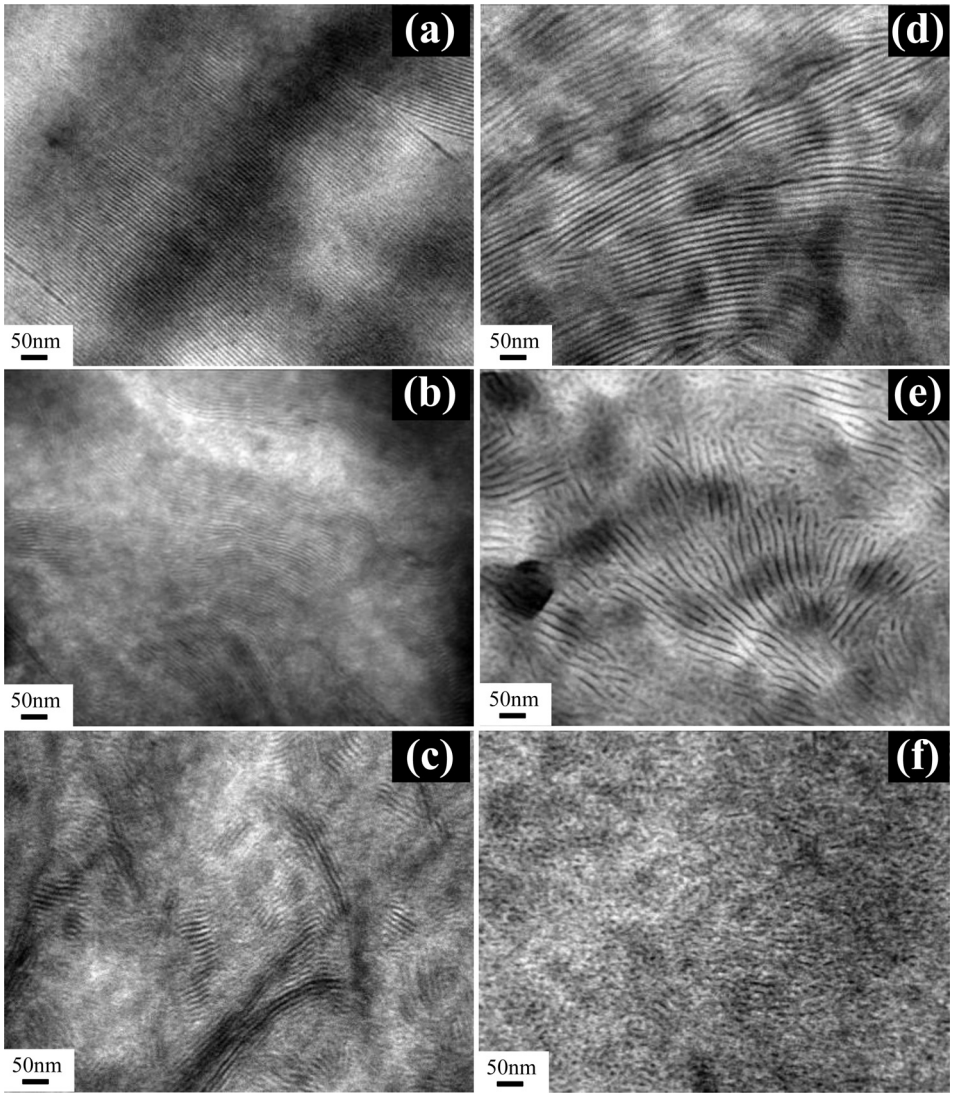


**Fig. 4.** TEM images of PPV-*b*-P2VP$_{0.3}$(DBSA)$_x$ rod–comb block copolymers with (a) $x = 0$, (b) $x = 0.5$, and (c) $x = 1.0$, and TEM images of PPV-*b*-P2VP$_{0.56}$(DBSA)$_x$ rod–comb block copolymers with (d) $x = 0$, (e) $x = 0.5$, and (f) $x = 1.0$. DEH-PPV domains stained with $RuO_4$ exhibit as a dark phase shown in the TEM images.

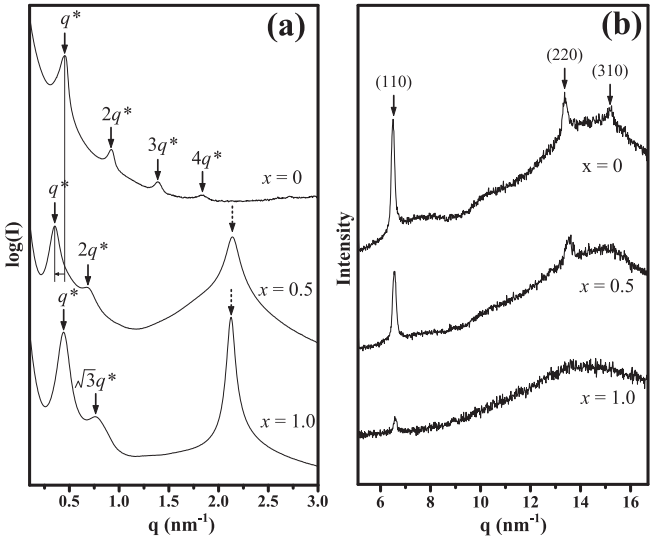


**Fig. 5.** The evolution of (a) SAXS and (b) WAXS patterns as a function of the number of DBSA molecules per vinyl pyridine repeating unit for the PPV-*b*-P2VP$_{0.56}$(DBSA)$_x$ complex.

Moreover, a further phase transformation is observed as the DBSA fraction was continuously increased. As the DBSA fraction was increased from $x = 0.5$ to $x = 1.0$, the SAXS profile shown in Fig. 5a for the PPV-*b*-P2VP$_{0.56}$(DBSA)$_{1.0}$ complex exhibits multiple scattering peaks with position at $1 : \sqrt{3}$ ratio relative to that of the first peak located at $q^* = 0.44$ nm$^{-1}$. This implies an existence of hexagonally packed microdomains with a shorter-range spatial order. The nanostructure of the PPV-*b*-P2VP$_{0.56}$(DBSA)$_{1.0}$ hybrid was also observed by using TEM. The TEM micrograph (Fig. 4f) showed that the DEH-PPV domains display a strip phase in PPV-*b*-P2VP$_{0.56}$(DBSA)$_{1.0}$, wherein the aggregates are slightly longer in one direction than the others.

In addition, analogous to the SAXS profiles of the PPV-*b*-P2VP$_{0.3}$(DBSA) hybrid system, a significant increase in the diffraction intensity and the sharpening of an additional peak at 2.1 nm$^{-1}$ (as indicated by a dotted arrow) are also observed, revealing the formation of a smaller length-scale lamellar mesophase organized by the P2VP(DBSA) comb phase. The way that DEH-PPV rods adopt to pack within the PPV-*b*-P2VP$_{0.56}$(DBSA)$_x$ hybrid nanodomains is also investigated by using WAXS. As shown in Fig. 5b, the first diffraction peak related to the (110) plane and located at around

6.5 $nm^{-1}$ corresponds to the lateral spacing between the DEH-PPV rods, which is unchanged from that of the previous PPV-*b*-$P2VP_{0.3}$ hybrid systems. The peak magnitude for DEH-PPV rod decreases dramatically with increasing DBSA fractions. Even though the phase transformation occurred from the broken lamellar phase to the hexagonally packed strip phase, the characteristic (110) peak position representing the distance for the rod–rod interaction remains unchanged. Therefore, based on the combined results of the TEM, SAXS and WAXS measurements, the hierarchical structure formed in the PPV-*b*-$P2VP_{0.56}(DBSA)_{1.0}$ complex where strip microdomains of DEH-PPV are embedded in the lamellar mesophase formed by the P2VP(DBSA) comb block can be schematically illustrated in Scheme 4b.

Furthermore, the correlation length, $D_{110}$, of the DEH-PPV-packed strip can be obtained from the primary scattering peak (110) by using Scherrer's equation [58]:

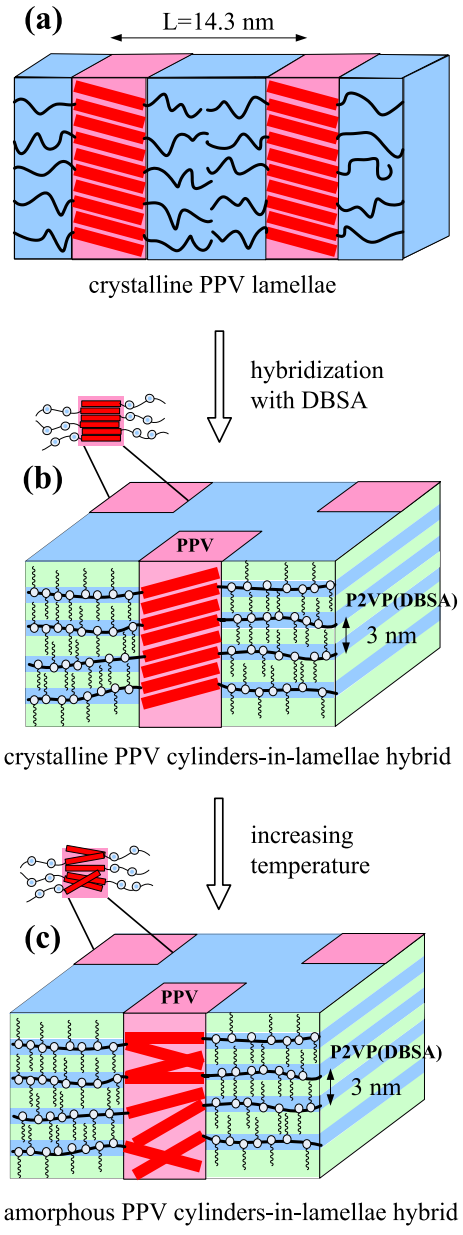


**Scheme 4.** (a) Lamellar morphology formed in neat PPV-*b*-$P2VP_{0.56}$ rod–coil block copolymer and hierarchical structure formed in PPV-*b*-$P2VP_{0.56}(DBSA)_{1.0}$ wherein strip microdomains of (b) crystalline and (c) amorphous DEH-PPV are embedded in the lamellar mesophase formed by P2VP(DBSA) comb block.

$$D_{hkl} = \frac{0.9\lambda}{\beta_{hkl}\cos\theta} \quad (1)$$

where $D_{hkl}$ is the crystallites size along the [hkl] direction, $\beta_{hkl}$ is the full width at half maximum of the [hkl] scattering peak, $\lambda$ is the wavelength of the X-rays and $2\theta$ is the scattering angle. The strip length consisting of DEH-PPV rods was estimated to be about 15.2 nm, which is in agreement with the estimate from its TEM image. Based on an approximate DEH-PPV rod diameter of 1 nm (~0.97 nm), this corresponds to ~15 DEH-PPV rods in each short strip aggregate.

### 3.3. Phase transformation

Since the anisotropic rod–rod interaction between π-conjugated DEH-PPV was found to be temperature dependent [51], simultaneously measured SAXS and WAXS experiments as a function of temperature were performed to investigate the effect of temperature on the self-assembling behavior of the solid and liquid crystalline structures of the PPV-*b*-P2VP(DBSA) hybrids.

At first, the phase transition of the neat PPV-*b*-$P2VP_{0.3}$ was observed by performing simultaneous SAXS and WAXS experiments as a function of different temperatures. As shown in Fig. 6a of the SAXS measurement and Fig. 6b of the WAXS measurement, PPV-*b*-$P2VP_{0.3}$ undergoes an ordered lamella-to-disorder transition and a smectic/isotropic transition simultaneously at ~190 °C. Analogous to the result of the evolution in the SAXS profiles of the neat PPV-*b*-$P2VP_{0.3}$ copolymer with temperature, the characteristic scattering peaks corresponding to the self-assembled lamellar phase of the neat PPV-*b*-$P2VP_{0.56}$ copolymer also disappears completely at ~190 °C (Fig. 7a), indicating the occurrence of the phase transition from the lamellar phase to a disordered phase. Concurrently, the WAXS diffraction peaks of the (110), (210), (220), and (310) planes associated with the liquid crystalline structure between DEH-PPV rods also disappear completely at 190 °C (Fig. 7b), indicating a smectic/isotropic transition. Therefore, it appears that the presence of the rod–rod interaction between DEH-PPV blocks may have the dominant effect on the formation and the stabilization of the lamellar structure for both neat block copolymers at temperatures below 190 °C.

Fig. 8a and b show the evolution of SAXS and WAXS patterns, respectively, as a function of temperature for the PPV-*b*-$P2VP_{0.3}(DBSA)_{1.0}$ hybrid. Compared with the result of its neat PPV-*b*-$P2VP_{0.3}$ block copolymer, the characteristic scattering peaks corresponding to the self-assembled lamellar phase of PPV-*b*-$P2VP_{0.3}(DBSA)_{1.0}$ hybrid disappear simultaneously with the anisotropic rod–rod interaction between π-conjugated DEH-PPV blocks at 190 °C, as indicated by the complete disappearance of the major (110) diffraction peak. Note that the diffraction peak at $q = 2.25\ nm^{-1}$ revealed in Fig. 8a, signifying the ionic/hydrogen bonding between P2VP and DBSA, remains significantly strong even at temperatures above 190 °C. In order to pin down the order-disorder transition temperature ($T_{ODT}$) for the self-assembled lamellar structure for the hybrids, the inverse of the primary SAXS scattering peak intensity as a function of the inverse temperature ($I_m^{-1}$ vs $T^{-1}$) can be plotted. As shown in Fig. 9a, $T_{ODT}$ for the PPV-*b*-$P2VP_{0.3}(DBSA)_{1.0}$ hybrid is estimated to be at around 190 °C, which is similar to that for the neat PPV-*b*-$P2VP_{0.3}$ block copolymer. Therefore, the presence of rod–rod interactions between DEH-PPV chains is found to have dominant effects on both the formation, as well as the stabilization, of the large-scale lamellar structure of PPV-*b*-$P2VP_{0.3}(DBSA)_{1.0}$ at temperatures around 180 °C. For temperatures above 180 °C, even though the ionic/hydrogen bonding between P2VP and DBSA still exists, the large-scale lamellar

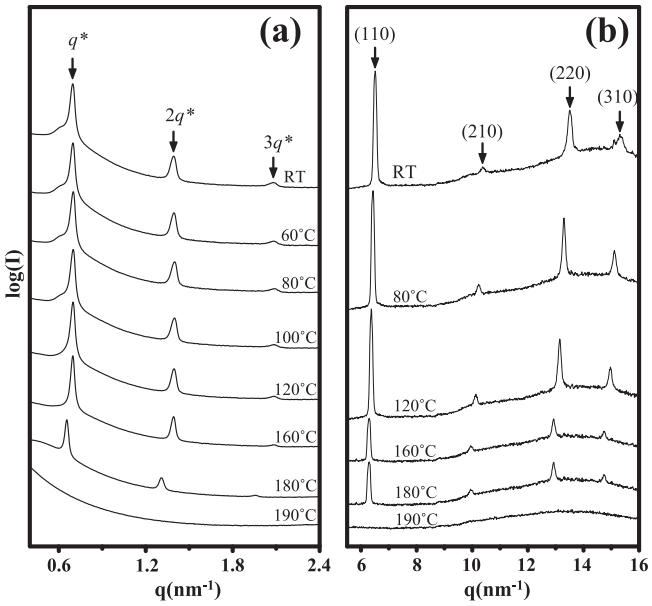


**Fig. 6.** Simultaneously measured (a) SAXS and (b) WAXS spectra as a function of temperature for the PPV-*b*-P2VP$_{0.3}$ block copolymer.

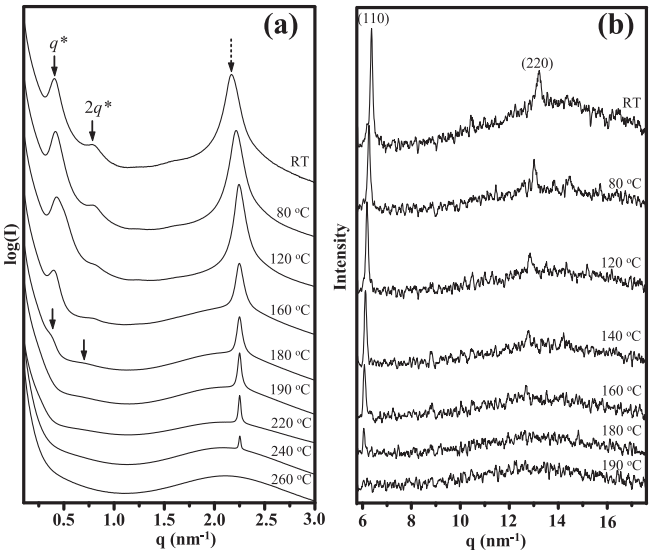


**Fig. 8.** Simultaneously measured (a) SAXS and (b) WAXS spectra as a function of temperature for the PPV-*b*-P2VP$_{0.3}$(DBSA)$_{1.0}$ complex.

structure disappears simultaneously with the rod–rod interaction of π-conjugated DEH-PPV blocks.

Additionally, we analyze the phase behavior of the PPV-*b*-P2VP$_{0.56}$(DBSA)$_{1.0}$ hybrids as a function of temperature. Fig. 10a and b show the temperature-dependent SAXS and WAXS patterns of PPV-*b*-P2VP$_{0.56}$(DBSA)$_{1.0}$ hybrid, respectively. Note that the crystalline peak at $q$ = 6.5 nm$^{-1}$ for the (110) plane for PPV-*b*-P2VP$_{0.56}$(DBSA)$_{1.0}$ hybrid disappears at a temperature of only ~120 °C, which is also lower than that (180 °C) for the neat PPV-*b*-P2VP$_{0.56}$ block copolymer that exhibited a 1D lamellar ordered structure. This indicates that the 2D confined strip phase for the PPV-*b*-P2VP$_{0.56}$(DBSA)$_{1.0}$ hybrid has a significant effect on how its

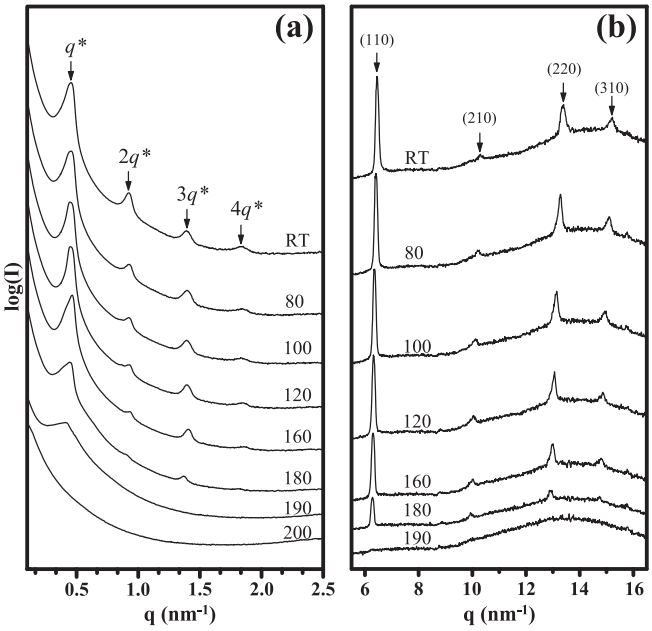


**Fig. 7.** Simultaneously measured (a) SAXS and (b) WAXS spectra as a function of temperature for the PPV-*b*-P2VP$_{0.56}$ block copolymer.

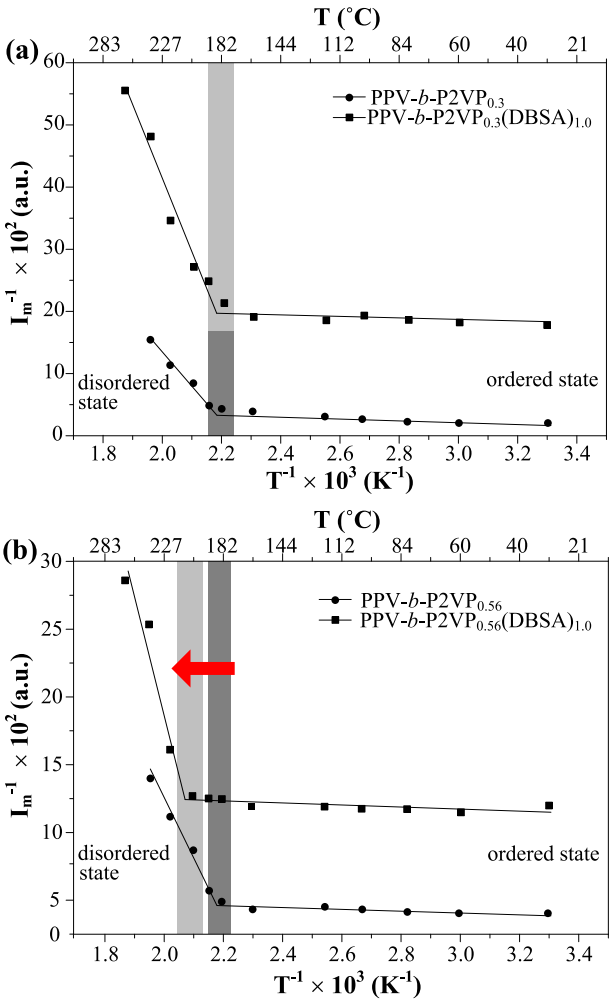


**Fig. 9.** $I_m^{-1}$ vs $T^{-1}$ plots of (a) PPV-*b*-P2VP$_{0.3}$ and PPV-*b*-P2VP$_{0.3}$(DBSA)$_{1.0}$ complexes, and (b) PPV-*b*-P2VP$_{0.56}$ and PPV-*b*-P2VP$_{0.56}$(DBSA)$_{1.0}$ complexes for the determination of $T_{ODT}$ associated with their P2VP(DBSA) comb block.

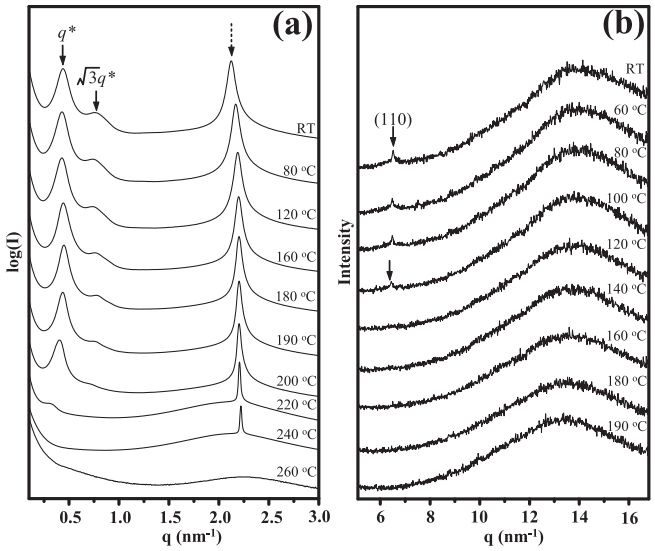


**Fig. 10.** Simultaneously measured (a) SAXS and (b) WAXS spectra as a function of temperature for the PPV-*b*-P2VP$_{0.56}$(DBSA)$_{1.0}$ complex.

π-conjugated DEH-PPV blocks pack. Despite the disappearance of the rod–rod interaction of π-conjugated DEH-PPV blocks, the self-assembled strip phase for PPV-*b*-P2VP$_{0.56}$(DBSA)$_{1.0}$ remains stable at temperatures higher than 180 °C. From Fig. 9b, the $T_{ODT}$ for the PPV-*b*-P2VP$_{0.56}$(DBSA)$_{1.0}$ hybrid is estimated to be at around 210 °C. It is also noted that DBSA attached to the P2VP blocks via both ionic and hydrogen bonding, with the latter being more predominate. The observed ODT of the strip mesophases may stem from the dissociation of the weaker hydrogen bonds; the ionically bonded DBSA remained intact even after the observed ODT has been reached (Fig. 10a). These strip domains were formed by the P2VP(DBSA) comb blocks with DBSA ionically bonded to P2VP [35]. Hence, the presence of the smaller-scale P2VP(DBSA) lamellar mesophase in the PPV-*b*-P2VP$_{0.56}$(DBSA)$_{1.0}$ complex may also have the governing effect on the formation and stabilization of the hexagonal strip structure. A schematic for the molecular packing of PPV-*b*-P2VP$_{0.56}$(DBSA)$_{1.0}$ at high temperatures (<180 °C) is shown in Scheme 4c. Correspondingly, the current study provides new insights into rod–comb block copolymer systems for controlling nanostructures at multiple length scales, as well as providing new strategies for future applications.

## 4. Conclusions

We investigated the self-assembly behavior of novel supramolecular rod–comb block copolymers formed by hybridization of an anionic surfactant DBSA with the PPV-*b*-P2VP rod–coil block copolymer as a function of DBSA bonded to P2VP. Two PPV-*b*-P2VP rod–coil block copolymers, each with DEH-PPV or P2VP as their major species, were used for the preparation of the hybrid samples. TEM and simultaneous SAXS/WAXS measurements as a function of temperature were used to investigate the effect of DBSA composition on the self-assembly behavior of the hybridized rod–comb system. For PPV-*b*-P2VP$_{0.3}$(DBSA)$_x$, the large-scale structure changes from lamellae with long-range order for the neat PPV-*b*-P2VP$_{0.3}$ block copolymer, to broken lamellae for the PPV-*b*-P2VP$_{0.3}$(DBSA)$_{1.0}$ complex. In order to prevent an excessive chain stretching of the P2VP(DBSA) blocks on the otherwise long-range ordered DEH-PPV lamellar phase, the PPV-*b*-P2VP$_{0.3}$(DBSA)$_{1.0}$ hybrid with an effective P2VP(DBSA) volume fraction of 0.72 still exhibited a lamellar phase with DEH-PPV forming a broken lamellar layer. For PPV-*b*-P2VP$_{0.56}$(DBSA)$_x$, the large-scale structure changes from lamellae, to broken lamellae, and eventually to the hexagonally packed strip phase as the amount of DBSA was increased from $x = 0$ to $x = 0.5$ and eventually to $x = 1.0$.

Upon heating, the crystalline phase of DEH-PPV in the PPV-*b*-P2VP$_{0.3}$(DBSA)$_{1.0}$ hybrid disappeared at temperatures above 190 °C and the large-scale broken lamellar phase persisted up to ~190 °C, at which point the rod–comb system underwent the order-to-disorder transition, indicating that the rod–rod interaction between DEH-PPV chains plays a key role in the formation and the stabilization of the broken lamellar structure. On the contrary, for PPV-*b*-P2VP$_{0.56}$(DBSA)$_{1.0}$, the rod–rod interaction disappeared early at 120 °C while the disordering of block copolymer microdomains occurred almost simultaneously at higher temperatures with that of the P2VP(DBSA) lamellar structure, indicating that the formation of the P2VP(DBSA) lamellar mesophase plays a critical role in forming and stabilizing this hexagonally packed strip structure. The current study may provide new guidelines for the organization of rod-comb block copolymer systems for future applications.

## Acknowledgments

The financial support of this work from the National Science Council of Taiwan is greatly appreciated. The authors would also like to thank all beamline staff and technical supports at the National Synchrotron Radiation Research Center of Taiwan for the X-ray measurements.

## Appendix A. Supplementary data

Supplementary data related to this article can be found online at http://dx.doi.org/10.1016/j.polymer.2014.01.056.

## References

[1] Bates FS, Fredrickson GH. Annu Rev Phys Chem 1990;41:525–57.
[2] Bates FS. Science 1991;251:898–905.
[3] Matsen MW, Schick M. Phys Rev Lett 1994;72:2660–3.
[4] Matsen MW, Bates FS. Macromolecules 1996;29:7641–4.
[5] Bates FS, Fredrickson GH. Phys Today 1999;52:32–8.
[6] Segalman RA. Mater Sci Eng R Rep 2005;48:191–226.
[7] Widawski G, Rawiso M, Francois B. Nature 1994;369:387–9.
[8] Hulvat JF, Sofos M, Tajima K, Stupp SI. J Am Chem Soc 2005;127:366–72.
[9] Van De Wetering K, Brochon C, Ngov C, Hadziioannou G. Macromolecules 2006;39:4289–97.
[10] Dai C-A, Yen W-C, Lee Y-H, Ho C-C, Su W-F. J Am Chem Soc 2007;129:11036–8.
[11] Lee Y-H, Chang C-J, Kao C-J, Dai C-A. Langmuir 2010;26:4196–206.
[12] Lee Y-H, Yen W-C, Su W-F, Dai C-A. Soft Matter 2011;7:10429–42.
[13] Yen W-C, Lee YH-, Lin J-F, Dai C-A, Jeng U-S, Su W-F. Langmuir 2011;27:109–15.
[14] Chang C-J, Lee Y-H, Chen H-L, Chiang C-H, Hsu H-F, Ho C-C, et al. Soft Matter 2011;7:10951–60.
[15] Lee Y-H, Yang Y-L, Yen W-C, Su W-F, Dai C-A. Nanoscale 2014;6:2194–200.
[16] Sauve G, McCullough RD. Adv Mater 2007;19:1822–55.
[17] Sirringhaus H, Tessler N, Friend RH. Science 1998;280:1741–4.
[18] Thompson BC, Frechet JMJ. Angew Chem Int Ed 2008;47:58–77.
[19] Woo CH, Thompson BC, Kim BJ, Toney MF, Frechet JMJ. J Am Chem Soc 2008;130:16324–9.
[20] Pryamitsyn V, Ganesan V. J Chem Phys 2004;120:5824–38.
[21] Matsen MW, Barrett C. J Chem Phys 1998;109:4108–18.
[22] Chen JT, Thomas EL, Ober CK, Mao GP. Science 1996;273:343–6.
[23] Chen JT, Thomas EL, Ober CK, Hwang SS. Macromolecules 1995;28:1688–97.
[24] Li CY, Tenneti KK, Zhang D, Zhang HL, Wan XH, Chen EQ, et al. Macromolecules 2004;37:2854–60.
[25] Ho C-C, Lee Y-H, Dai C-A, Segalman RA, Su W-F. Macromolecules 2009;42:4208–19.
[26] Lee M, Cho BK, Kim H, Yoon JY, Zin WC. J Am Chem Soc 1998;120:9168–79.
[27] Radzilowski LH, Carragher BO, Stupp SI. Macromolecules 1997;30:2110–9.
[28] Cho BK, Chung YW, Lee M. Macromolecules 2005;38:10261–5.
[29] Ryu JH, Oh NK, Zin WC, Lee M. J Am Chem Soc 2004;126:3551–8.
[30] Hartikainen J, Lahtinen M, Torkkeli M, Serimaa R, Valkonen J, Rissanen K, et al. Macromolecules 2001;34:7789–95.

[31] Korhonen JT, Verho T, Rannou P, Ikkala O. Macromolecules 2010;43:1507–14.
[32] Chiang W-S, Lin C-H, Yeh C-L, Nandan B, Hsu P-N, Lin C-W, et al. Macromolecules 2009;42:2304–8.
[33] Chen H-L, Lu J-S, Yu C-H, Yeh C-L, Jeng U-S, Chen W-C. Macromolecules 2007;40:3271–6.
[34] Nandan B, Lee C-H, Chen H-L, Chen W-C. Macromolecules 2006;39:4460–8.
[35] Nandan B, Lee C-H, Chen H-L, Chen W-C. Macromolecules 2005;38:10117–26.
[36] Valkama S, Ruotsalainen T, Nykanen A, Laiho A, Kosonen H, ten Brinke G, et al. Macromolecules 2006;39:9327–36.
[37] Ruokolainen J, tenBrinke G, Ikkala O, Torkkeli M, Serimaa R. Macromolecules 1996;29:3409–15.
[38] Ikkala O, Ruokolainen J, Tenbrinke G, Torkkeli M, Serimaa R. Macromolecules 1995;28:7088–94.
[39] Geng CZ, Su JJ, Han SJ, Wang K, Fu Q. Polymer 2013;54:3392–401.
[40] Liu JG, Sun Y, Zheng LD, Geng YH, Han YC. Polymer 2013;54:423–30.
[41] Zheng JF, Zhang HY, Zhao ZG, Han CC. Polymer 2012;53:546–54.
[42] Sun YS, Chien SW, Liou JY, Su CH, Liao KF. Polymer 2011;52:1180–90.
[43] ten Brinke G, Ruokolainen J, Ikkala O. Hydrogen Bonded Polymers 2007;207:113–77.
[44] Kato T, Mizoshita N, Kishimoto K. Angew Chem Int Ed 2006;45:38–68.
[45] Valkama S, Kosonen H, Ruokolainen J, Haatainen T, Torkkeli M, Serimaa R, et al. Nat Mater 2004;3:872–6.
[46] Valkama S, Ruotsalainen T, Kosonen H, Ruokolainen J, Torkkeli M, Serimaa R, et al. Macromolecules 2003;36:3986–91.
[47] Ikkala O, ten Brinke G. Chem Commun; 2004:2131–7.
[48] Ikkala O, ten Brinke G. Science 2002;295:2407–9.
[49] Kosonen H, Valkama S, Ruokolainen J, Torkkeli M, Serimaa R, ten Brinke G, et al. Eur Phys J E 2003;10:69–75.
[50] Osuji C, Chao CY, Bita I, Ober CK, Thomas EL. Adv Funct Mater 2002;12:753–8.
[51] Olsen BD, Shah M, Ganesan V, Segalman RA. Macromolecules 2008;41:6809–17.
[52] Olsen BD, Segalman RA. Macromolecules 2007;40:6922–9.
[53] Olsen BD, Segalman RA. Macromolecules 2005;38:10127–37.
[54] Sary N, Rubatat L, Brochon C, Hadziioannou G, Ruokolainen J, Mezzenga R. Macromolecules 2007;40:6990–7.
[55] Kretzschmann H, Meier H. Tetrahedron Lett 1991;32:5059–62.
[56] Olsen BD, Jang SY, Luning JM, Segalman RA. Macromolecules 2006;39:4469–79.
[57] Olsen BD, Segalman RA. Macromolecules 2006;39:7078–83.
[58] Huang P, Guo Y, Quirk RP, Ruan JJ, Lotz B, Thomas EL, et al. Polymer 2006;47:5457–66.